Sixth International Symposium on Turbulence and Shear Flow Phenomena
Seoul, Korea, 22-24 June 2009

TRANSIENT DYNAMICS OF THE FLOW AROUND A NACA 0015 AIRFOIL USING FLUIDIC VORTEX GENERATORS

Wei Long Siauw, Jean-Paul Bonnet, Jean Tensi, Laurent Cordier
Laboratoire d'Etudes Aérodynamiques
University of Poitiers, ENSMA, CNRS
43 rue de l'aérodrome, F-86036 Poitiers, France
jean-paul.bonnet@univ-poitiers.fr

Bernd R. Noack
Berlin Institute of Technology MB1
Straße des 17. Juni 135,
D-10623 Berlin, Germany
bernd.r.noack@tu-berlin.de

Louis Cattafesta
Florida Center for Advanced Aero-Propulsion (FCAAP)
Department of Mechanical and Aerospace Engineering
University of Florida
231 MAE-A, Gainesville, FL 32611, USA
cattafes@ufl.edu

ABSTRACT

The unsteady activation/deactivation of fluidic vortex generators on a NACA 0015 airfoil is studied to understand the transient dynamics of flow separation control. The Reynolds number is high enough and the boundary layer is tripped, so the boundary layer is fully turbulent. Conditional PIV of the airfoil wake is obtained phase-locked to the actuator trigger signal, allowing reconstruction of the transient processes. When the flow is impulsively attached, the velocity field in the near wake exhibit a complex transient behavior associated with the formation and shedding of a starting vortex. This confirms results in the literature obtained in comparable configurations. The separation dynamics when actuation is stopped is a more gradual process. The Proper Orthogonal Decomposition reveals low-dimensional transient dynamics, with 98% of the fluctuation energy captured by the first four modes. The behavior is quantitatively well captured by a 4-dimensional dynamical system with the corresponding mode amplitudes. Analysis accurately determines typical time scales for attachment and separation processes are $T^+ = \Delta t U_\infty / L_{sep} = 10$ and 20 in conventional non dimensional values. This study adds to experimental investigations of this scale with essential insights for the targeted closed-loop control.

INTRODUCTION

The study of active control of flow separation via fluidic actuators has been undertaken by several researchers to suppress and delay flow separation over an airfoil pitched at high incidence. Most research focuses on open-loop pre-determined control using steady/unsteady jets without consideration of the state of the flow field. Examples of steady jet control techniques can be found in the work of Eldredge and Bons (2004), Sondergaard et al. (2002), Erm (2001), and Johnston and Compton (1992). In the case of the introduction of unsteady jet actuation, readers can refer to, for example, Hansen and Bons (2006), Seifert et al. (2004), and Amitay and Glezer (2002a). Most of these studies target the steady or quasi-steady state performance of lift enhancement and drag reduction at relatively low chord Reynolds number (typically less than 0.5 million). Closed-loop airfoil separation control has been studied at relatively low Reynolds number by Tian et al. (2006) and Pinier et al. (2007).

Detailed studies concerning the transient process of flow attachment and separation in response to a synthetic jet actuator have been performed by Darabi and Wygnanski (2004a and b); and Amitay and Glezer (2002b, 2006). Mathis et al. (2009) performed a similar study using a steady jet to provoke separation to enhance mixing.

Table 1 shows that the typical time scales (non dimensionalized by the length of the separation zone and the external velocity) to achieve attachment and separation are quite different. It should be emphasized that, for the two first cases, the flow is naturally separated and the actuation enforces flow attachment. In Mathis et al., the flow is naturally attached and then the actuators promote separation.

Table 1: Typical Separation/Attachment Time Scales.

Authors	Amitay and Glezer (2002b)	Darabi and Wygnanski (2004a)	Mathis et al. (2009)
Test Configuration	Modified wing profile	Generic Flap	Beveled Splitter Plate
Reynolds Number	3.1 x 10^5	1.24 x 10^5	1.44 x 10^5
Actuator Type	Synthetic jet	Synthetic jet	Steady jet
C_μ	10^{-3}	10^{-4}	10^{-2}
$\Delta T+$ (attachment)	~ 9.5	16-70 (16 is the optimal value)	5
$\Delta T+$ (separation)	~ 14	20	25

So far, relatively little attention has been paid to the transient aspects of the problem, which can be important if we consider that any closed loop control necessitates the knowledge of the typical time scales and the associated

dynamical behaviour of the entire process. From the three examples given above, it appears that no universal value exists. These discrepancies can be attributed to several origins. First, the physics of the process of separation/attachment is entirely dependent on whether the initial state is attached or separated. Second, the mode of actuation is generally different in each study. However, the transient separation process may not depend on the actuation approach. Thirdly, the flow configuration (wing, flap or bevel) and Reynolds number effects cannot be neglected at low Reynolds numbers. Lastly it should be emphasized that the determination of the typical time scales is not straightforward and can correspond to different definitions.

Time scales are key order parameters in closed-loop control strategies. Reduced order modeling (ROM) is a vital enabler in most closed loop control systems. Ausseur et al. (2006a,b) and Perret et al. (2006) identify reduced order models to predict the experimental flow dynamics in terms of POD mode for different uncontrolled configurations (see Cordier et al. (2009) for a recent paper summarizing the calibration approaches). The procedures involve solving for the coefficients belonging to a set of dynamical equations, which are hypothesized to describe a set of reduced order dynamics derived from the dominant POD modes of experimental data. Depending on the phenomenological behavior of the flow, the dynamical equations can be first- or higher-order. In the current work, the two-point velocity correlation tensor has been used as the kernel for the POD. This is the common choice in the literature but other kernels can be used, such as correlation of vorticity (Ausseur et al., 2006b). Recently, a pressure sensor array has been used to estimate flow fields by using linear stochastic estimation (LSE) (Pinier et al. 2007). Stalnov et al. (2007) used signals from a surface mounted hot-film array to estimate the structures in the wake of a D-shaped profile. Such methods could form the basis of a control strategy for closed-loop separation control.

The current study concerns the transient dynamics of attachment and separation over a NACA 0015 airfoil operating at a chord Reynolds number of about 1 million in response to the deployment and removal of an array of 44 steady pitched (30^o) and skewed (60^o) fluidic vortex generators (FVGs) positioned at x/c of 0.3. The chosen flow condition is such that jet deployment corresponds to complete flow attachment over the airfoil; jet removal will cause flow separation up to an extent defined by the uncontrolled separated state. This paper utilizes conditional PIV to probe the transient flow dynamics. In particular, the FVGs are pulsed at a frequency of 1 Hz in an "on-off" manner in order to enable conditional sampling for both experiments involving PIV and hot wire anemometry.

The objective in the current work focuses on providing a description of the physics of flow attachment and separation in response to the deployment and removal of the FVGs. This includes:

(1) the estimation of the time scales of flow attachment and separation; and
(2) reduced order modelling based on conditionally averaged PIV data.

EXPERIMENTAL DETAILS

The closed-loop wind tunnel used for the study has a test section size of 2.4 m by 2.6 m with a turbulence intensity of 0.5% at 40 m/sec. A 0.35m chord, 2.4 m span NACA 0015 model is installed in the test section. To trip the boundary layer, 80 μm carborandum grit is applied at 0.4% of the chord from the leading edge. The test condition corresponds to a chord Reynolds number of approximately 1 million and an incidence angle of 11^o.

Fluidic vortex generators are deployed through an array located at 30% chord of 44 x 1 mm diameter orifices, spaced 15 mm apart in the spanwise direction. This array occupies the central one third spanwise portion of the airfoil. As shown in Figure 1, the FVGs are pitched 30^o and yawed at 60^o. The peak velocity of the jet is set at about 200 m/s, corresponding to a C_μ of 0.67%.

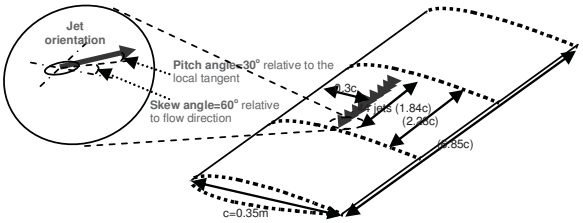

Figure 1. FVGs installed at 30% of chord length.

To characterize the transients, the FVGs deployment system must respond much faster than the characteristic times of attachment and separation. This is achieved by installing four ASCO solenoid valves (CM25-5W) inside the airfoil model, such that 11 orifices are controlled by 1 valve. These valves possess an average response time (time to open/close the valve) of about 3 ms (Siauw 2008). The valves are operated by controlling the on/off state of a solid state relay that is triggered via a square wave.

A LaVision PIV system is used to study the transient dynamics of the wake (see Figure 2) in response to flow attachment and separation over the NACA 0015 airfoil via deployment and deactivation of the VFGs, respectively. The system software synchronizes laser pulsing and image acquisition from a camera system possessing a resolution of 1350 by 1048 pixels using the valve external trigger signal (1 Hz) for conditional sampling. A laser pulsed with a time interval of 200 μs is used. The cross-correlation technique is employed using an interrogation window size of 16 by 16 pixels with a 75% overlap ratio.

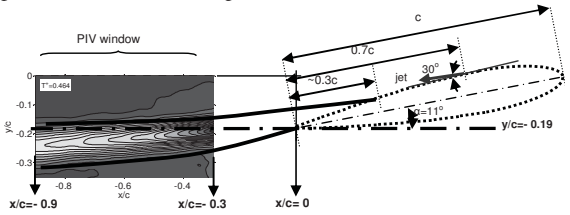

Figure 2. Schematic of the PIV window in the airfoil wake.

Figure 3 illustrates the conditional sampling technique employed during FVG deployment, in which 300 independent snapshots are obtained at 40 different time delays relative to the start of the transient. The phase-locked ensemble averaged velocity field is

$$\left\langle U_i(\vec{X},\Delta\tau)\right\rangle = \sum_{m=1}^{N=300}\frac{\left[U_i(\vec{X},\Delta\tau+mT)\right]}{N} \qquad (1)$$

where $\Delta\tau$ is the time delay relative to the start of the trigger signal and T is the period of the square wave, which is chosen to be sufficiently long for the flow to reach an asymptotic steady state.

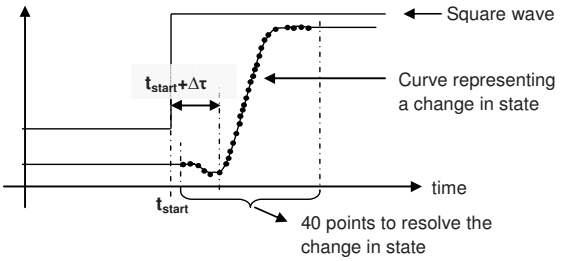

Figure 3. Illustration of conditional PIV sampling to characterize the change of flow state after FVG deployment.

Important information about the transient dynamics can be retrieved at each time delay by analyzing the statistics of the 300 independent snapshots for time delay. Conditional POD can be applied to this data set according to:

$$U_i(\vec{X},t) = \bar{U}_i(\vec{X},t) + \sum_n \lambda^{(n)} a^{(n)}(t) \Psi_i^{(n)}(\vec{X}) \qquad (2)$$

In the current study, the mean velocity field, which consists of an ensemble of 300 instantaneous snapshots of the wake flow, is subtracted from each snapshot at a particular time delay. A dynamical system that describes the uncontrolled or controlled flow can be deduced by projecting the POD modes onto the Navier-Stokes equation via the Galerkin method (Holmes et al. 1997). But it is difficult to construct a reduced order model describing the flow transient during an experiment due to deployment or removal of control. More complex methods that utilize a Galerkin projection of interpolated modes between flow transitions during control can be used instead; this has been implemented by Tadmor et al. (2007) and Noack et al. (2003).

ROM of Conditional Averaged Data. A reduced order model based on the temporal modes $a^{(n)}$ extracted from equation (2) can be expressed as a set of first-order state equations

$$\frac{da^{(n)}(t)}{dt} = A_{mn} a^{(n)}(t) + B_n b(t) \qquad (3)$$

where A_{mn} and B_n are the coefficients associated with the temporal modes and suitably scaled actuation signal, respectively. Equation (3) corresponds to the state space model of a linear time-invariant system. In the current work, the control command $b(t)$ is approximated by the velocity fluctuations from a hotwire positioned 3 mm from a FVG orifice with the tunnel on. The problem of reduced order modeling becomes simply a matter of solving a set of linear equations (i.e. solve for A_{mn} and B_n) for the known $a^{(n)}$ and $b(t)$.

In order to obtain an efficient reduced order model, we minimize the number of modes required by using the conditional averaged data, which removes information due to the fine scale turbulence. The significant information that remains is associated with large scale structures in response to the control transient. Once the linear coefficients (A_{mn} and B_n) are determined, we can simulate the system dynamics by integrating equation (3):

$$a^{(n)}(t) = \int \left[A_{mn} a^{(n)}(t) + B_n b(t) \right] dt \qquad (4)$$

A 5th order Runge-Kutta integration scheme is used for numerical integration. Such a model is useful as an exploratory model to study the transient dynamics if there are changes to the initial condition and actuation signal.

UNSTEADY BEHAVIOUR

Changes in mean and Turbulent Velocity Fields

The conditional averaging process allows for the analysis of the time evolution of the wake. The time evolution is obtained from equation (1).

Attachment Phase

When the FVGs are deployed, it can be observed from the contours of U/U_∞ velocity plotted in Figure 4 that the wake starts to undulate between T^+=6.96 and 8.82 without much increase in size. The wake starts to increase in size from T^+=8.82 to T^+=10.2; this increase is rapid and progresses from the upstream to downstream position. This interval corresponds to the initial increase of drag associated with the "starting vortex" passage observed by several authors (e.g., Amitay and Glezer 2002b). From T^+=10.7 to 13.5, the wake reduces in size progressively from upstream to downstream. After this, the wake tends asymptotically to the final reduced size. During the whole process, the velocity in the region of the wake axis has been redistributed such that the initially higher velocity deficit at x/c=-0.3 is reduced (i.e. higher velocity) and, conversely, the initially lower velocity deficit at x/c=-0.9 is increased (i.e. lower velocity). The overall result is a reduction in drag.

The transient phenomenon is also related to the complex turbulence behaviour depicted in Figure 5, in which the shear stress $\langle u'v' \rangle$ contours are plotted. The shear stress is more intense in the upstream position at T^+=0.464 (i.e., before the effects of the jet deployment is felt). From T^+ = 6.69 to 8.82, the shear stresses increase in intensity in the downstream direction. At T^+=10.2, the high shear stress region begins to decrease from the upstream direction. The negative shear stress region (wake bottom) has been evacuated from the PIV window more quickly than the positive shear stress regions (wake top); this occurs from T^+ = 11.1 to 13.9. Considering the shear stress distribution at T^+=0.464 as the reference profile at x/c=-0.85, the shear stress increases by more than 50% during the transient and decreases by about 50% at T^+=16.3, when the flow has been attached over the airfoil.

Separation Phase

When the FVGs are deactivated, the flow starts to separate and returns to its baseline configuration. The mean streamwise velocity contours are plotted in Figure 6. The velocity field shows a gradual enlargement of the wake and an upward shift of the wake axis which is similar to the jet deployment process. However, the undulation (wave like behaviour) observed in the attachment phase in the wake is not observed here. Thus, the passage of large eddies with spatial scales larger than that of the uncontrolled vortex streets in the downstream direction is probably not present.

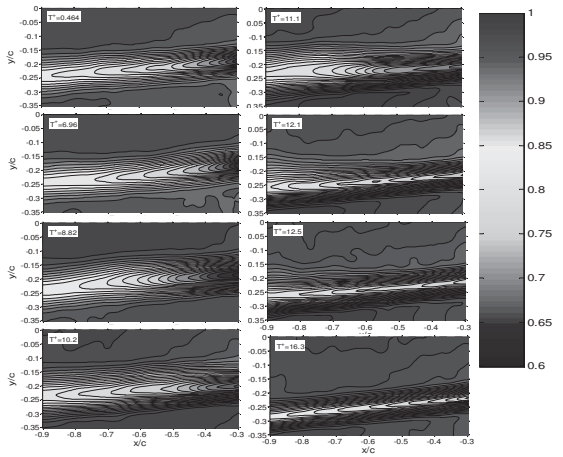

Figure 4. Evolution of the mean velocity in the airfoil wake during the attachment process.

This statement is substantiated in the analysis of the turbulent shear stress plotted in Figure 6. Based on the contour levels along the wake axis, the velocity deficit decreases at the downstream position at x/c=-0.85. The inverse is observed at the upstream position at x/c=-0.3.

The movement of the wake axis proceeds by a slight downward movement followed by a gradual upward movement towards its asymptotic position. The estimated drag coefficients using the curve-fitted wake profiles (not presented here, see Siauw 2008 for details) show that there is a slight decrease followed by a gradual increase. The decrease in C_d is due to a decrease in the size of the wake between T+=11.8 and 13.6 This is dramatically different from the jet deployment process, during which there is a rapid increase in C_d before it reduces to its asymptotic level with a lower C_d compared to the uncontrolled state.

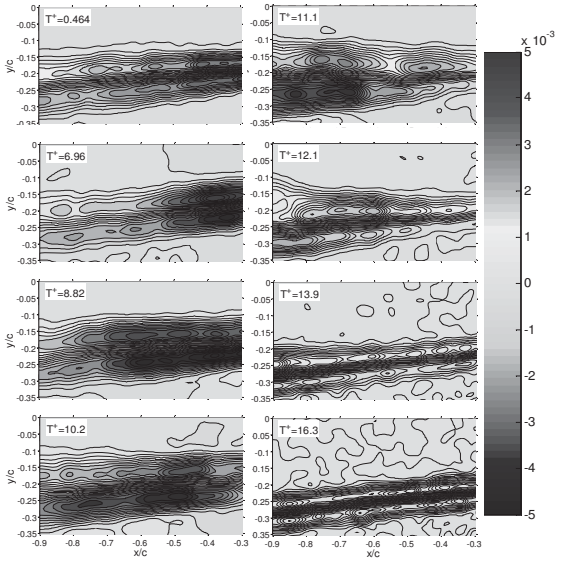

Figure 5. Evolution of the turbulent shear stress in the airfoil wake during the attachment process.

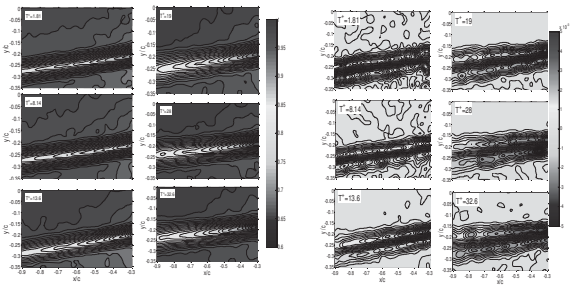

(a) (b)

Figure 6. Evolution of the streamwise velocity (a) and turbulent shear stress (b) in the airfoil wake during the FVGs removal (separation) process.

POD analysis

First we analyze the time instant at T+=0.464 when the wake has not yet been influenced by the deployment of the FVGs. This will serve as a reference for the dynamical system analysis. Figure 7 reveals the length scales associated with vortex shedding in the wake for the first and second modes of the POD. A length scale corresponding to 0.18c and 0.36c can be determined from the first and second mode, respectively.

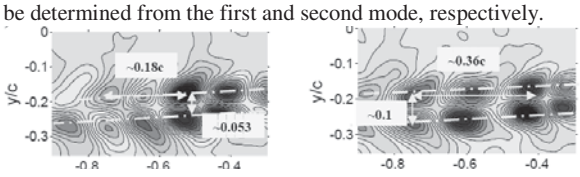

Figure 7. Two first POD modes for the uncontrolled configuration (left: mode 1, right: mode 2).

For the transient dynamics study, the modes are constructed with respect to the initial state of the flow at T+=0.464. Thus, the spatial modes are interpreted as changes with respect to the conditional averaged velocity field at T+=0.464 and not interpreted in the usual sense of a turbulent fluctuation. There is a rapid convergence of the cumulative eigenvalues as shown in Figure 8 where four modes are sufficient to capture 98% of the flow transient energy during jet deployment. The dynamical system will then be analyzed with the 4 first modes.

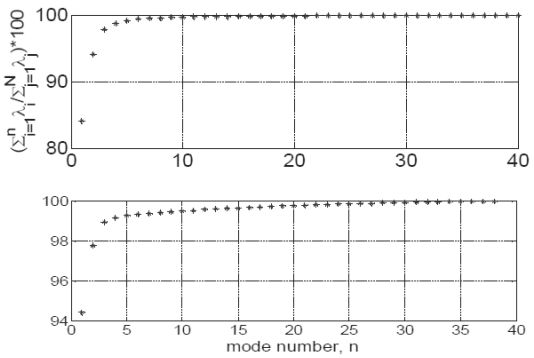

Figure 8. Convergence of the POD modes for the attachment (top) and separation (bottom) processes.

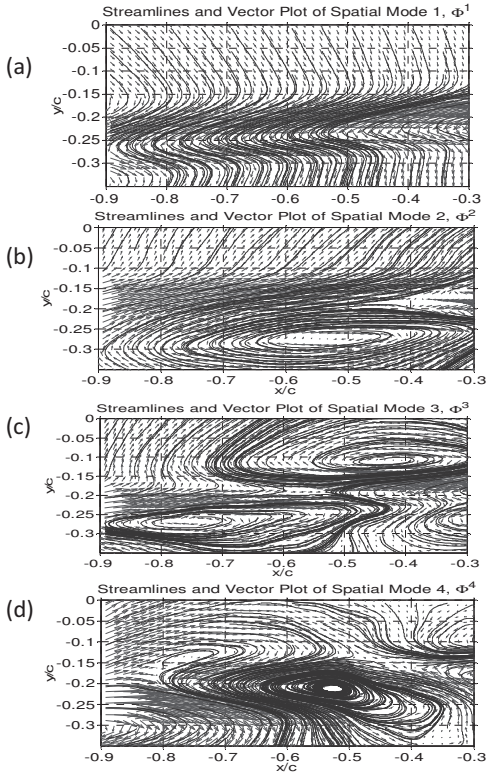

Figure 9. Plot of the in-plane streamlines of spatial modes from the conditional POD for the jet deployment process: (a) first mode; (b) second mode; (c) third mode; and (d) fourth mode.

The corresponding eigenfunctions (spatial modes) for the FVGs deployment (attachment phase) are shown in Figure 9. Spatial mode 1 corresponds to the mode that is responsible for the change in state from a larger wake to a smaller wake. It can be viewed as the dominant mode that modifies the momentum distribution in the region of the uncontrolled wake axis into that of the controlled wake. In the process, the size and position of the wake axis will be modified. Mode 2, which manifests itself as a large eddy, could be interpreted as the mode that causes the flow to displace slightly upwards before directing the flow downwards. Mode 3 is interpreted as the distortion of the conditional averaged velocity field due to the passage of large eddies.

Four modes have been used to model the transient process. The temporal modes $a^{(n)}(t)$ (n=1 to 4) as shown in Figure 10 are substituted into (3). The acceleration term $da^{(n)}/dt$ is computed by a first order finite difference approximation; thus, we have an over-determined set of linear equations (40 linear equations to determine 5 variables) for each mode. The coefficients A_{mn} and B_n are then solved by the method of least squares. The actuation signal b(t), measured by a hotwire at the exit of the jet orifice, has been used with a time delay associated with the convection time for the signal to reach the PIV window during the solution process; this is approximated by taking the total distance from the position of the orifice to the mid position of the PIV window: $(0.7c+0.6c)/(0.91U_\infty)=0.0117$ s, equivalent to a T+=4. The initial conditions of all 4 temporal modes are set to zero. In order to validate the model, the $a^{(n)}(t)$ can be predicted by integrating (4). As shown in Figure 10, the modeled $a^{(n)}(t)$ deduced from POD are in close agreement.

In terms of the temporal evolution as shown in Figure 10, it is clear that the first temporal mode describes a change between two states (jet activated and deactivated states) with a typical time T^+~10. The second mode, which peaks at T^+=10.2, describes the movement of a virtual large eddy (2nd spatial mode) that starts to appear at about T^+=6.69 and diminishes to a small value at T^+=15.

The transient of the separation phase (when the FVGs are deactivated) is represented by the first temporal mode as shown in Figure 11. In contrast to the deployment case, the first temporal mode takes about T+=20 to complete the change in state. This is twice that of the jet deployment case. The second mode describes the initial downward movement of the wake before moving back upwards. The contour level at the wake axis becomes more negative (from T+=4.52 to 13.6) before assuming less negative values (from T+=13.6 to 36.2). Clear similarities are observed in the first and second modes (both spatial and temporal) when compared with the jet deployment case. Thus, the transient dynamics for these two different flow control processes, both of which describe a change between two states, are similar when T+ are scaled by the respective time intervals for the transient processes.

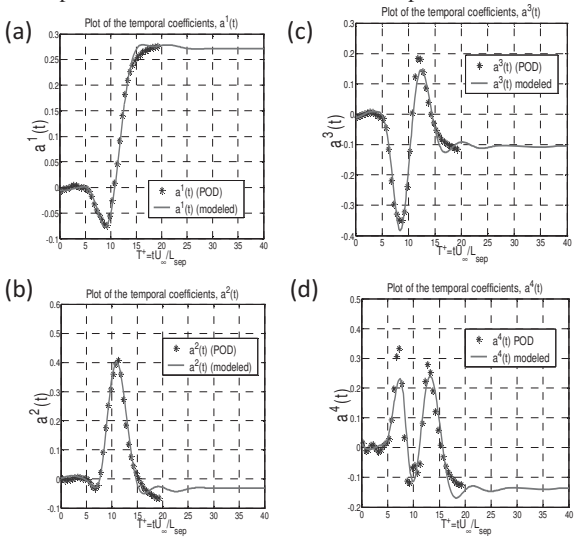

Figure 10. Plot of the temporal modes from the conditional POD for the jet deployment process compared to the modelled coefficients using a first order response function: (a) first mode; (b) second mode; (c) third mode; and (d) fourth mode.

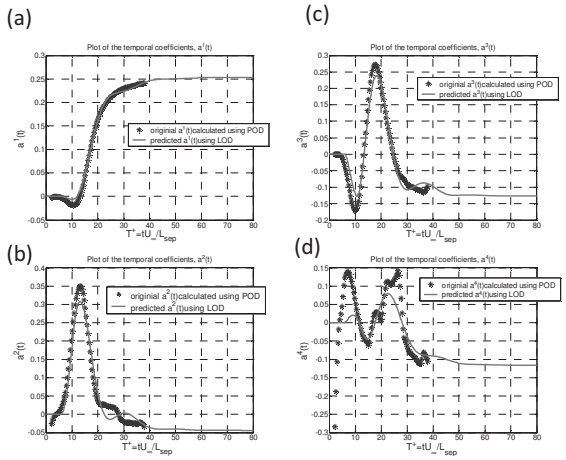

Figure 11. Plot of the temporal modes from the conditional POD for the jet removal process compared to the modelled coefficients using a first order response function: (a) first mode; (b) second mode; (c) third mode; and (d) fourth mode.

CONCLUDING REMARKS

The transient dynamics of attachment and separation on a NACA 00015 at high Reynolds number using impulsive FVGs are studied. The flow is analyzed via conditional PIV measurements in the near wake of the airfoil. The attachment process shows a strong transient effect associated with passage of a starting vortex. On the other hand, when the FVGs are deactivated, a more progressive separation process is observed. Simple direct analysis of the phase-locked PIV velocity field is insufficient to unambiguously determine the time scales. Conditional POD analysis is used for this purpose. It shows a rapid convergence in both processes, requiring only 4 modes to capture 98% of the flow transient energy. Analysis of the results provides estimates of the typical dimensionless time scale for attachment of $T^+ \sim 10$. It should be noted that this value is in agreement with the airfoil experiment of Amitay and Glezer (2002b), but less comparable with the ramp results of Darabi and Wygnanski (2004a). The discrepancy with the second reference can be attributed both to Reynolds number and geometric effects. In contrast, the time interval for separation ($T^+ \sim 20$) when the jets are deactivated lies within the accepted results, suggesting this time scale is approximately independent of actuator dynamics, geometry, and Reynolds number.

REFERENCES

Amitay M. and Glezer A. (2002a), "Role of Actuation Frequency in Controlled Flow Reattachment Over a Stalled Airfoil", *AIAA J.*, Vol. 40, No. 2, pp. 209-216.

Amitay M. and Glezer A. (2002b), "Controlled Transient of Flow Reattachment Over Stalled Airfoils", *Int. J. Heat Fluid Fl.*, Vol. 23, pp. 690-699.

Amitay M. and Glezer A. (2006), "Flow Transients Induced on a 2D Airfoil by Pulse-Modulated Actuation" Exp. Fluids, Vol. 40, pp. 329-331.

Ausseur J., Pinier J. T., Glauser M. N. and Higuchi H. (2006a). "Experimental Development of a Reduced Order Model for Flow Separation Control", AIAA 2006-1251.

Ausseur J., Pinier J. and Glauser M. N. (2006b). "Flow Separation Control Using a Convective Based POD Approach", AIAA 2006-3017.

Cordier L., Abou El Majd B. and Favier J. (2009), "Calibration of POD Reduced-Order Models using Tikhonov Regularization", accepted for publication in Int. J. Num. Meth. in Fluids.

Darabi A. and Wygnanski I. (2004a), "Active Management of Naturally Separated Flow Over a Solid Surface. Part 1. The Forced Reattachment Process", *J. Fluid Mech.*, Vol. 510, pp. 105-129.

Darabi A. and Wygnanski I. (2004b), "Active Management of Naturally Separated Flow over a Solid Surface. Part 2. The Separation Process", *J. Fluid Mech.*, Vol. 510, pp. 131-144.

Eldredge R. and Bons J. (2004). "Active Control of a Separating Boundary Layer with Steady Vortex Generating Jets - Detailed Flow Measurements". AIAA 2004-751.

Erm L. P. (2001). "Parametric Study of Jet/Vortex Interactions in AMRL Water Tunnel", Defense Science and Technology, DSTO-TR-1209.

Hansen L. and Bons J. (2006). "Flow Measurements of Vortex Generator Jets in Separating Boundary Layer", *J. Propul. Power*, Vol. 2, No. 3, pp. 558-565.

Holmes P. J., Lumley J. L., Berkooz G., Mattingly J. C. and Wittenberg R. W. (1997), "Low-Dimensional Models of Coherent Structures In Turbulence", *Physics Reports*, Vol. 287, pp. 337-384.

Johnston J. P. and Compton D. C. (1992). "Streamwise Vortex Production by Pitched and Skewed Jets in a Turbulent Boundary Layer", *AIAA J.*, Vol. 30, No. 3, pp. 640-647.

Mathis R, Lebedev A., Collin E, Delville J, and Bonnet J. P. (2009), "Experimental Study of Transient Forced Turbulent Separation and Reattachment on a Bevelled Trailing Edge", *Exp. Fluids*, 46 (1), pp. 131-146.

Noack B. R., Afanasiev K., Morzynski M., Tadmor G. and Thiele F. (2003),"A Hierarchy of Low-Dimensional Models for the Transient and Post-Transient Cylinder Wake", *J. Fluid Mech.,* Vol. 497, pp. 335–363.

Perret L., Collin E. and Delville J. (2006), "Polynomial Identification of POD Based Low-Order Dynamical System", *J. Turbul.*, Vol. 7, No. 17, pp. 17-33.

Pinier J., Ausseur J., Glauser M.N. and Higuchi H. (2007). "Proportional Closed-Loop Feedback Control of Flow Separation", *AIAA J.,* Vol. 45. No. 1, pp. 181-190.

Seifert A., Greenblatt D. and Wygnanski I. (2004). "Active Separation Control: An Overview of Reynolds and Mach Numbers Effects", *Aerosp. Sci. Technol.*, Vol. 8, pp. 569–582.

Sondergaard R., Rivir R. B. and Bons J. P. (2002). "Control of Low-Pressure Turbine Separation Using Vortex Generators", *J. Propul. Power*, Vol. 18, No. 4, pp. 889-895.

Siauw W.L., 2008, "Transient process of separation and attachment over a NACA 0015 airfoil controlled by fluidic vortex generators", Ph.D. Thesis, University of Poitiers, France.

Stalnov O., Palei V., Fono I, Cohen K. and Seifert A. (2007). "Experimental Estimation of a D-Shaped Cylinder Wake Using Body Mounted Sensors", *Exp. Fluids*, Vol. 42, pp. 531-542.

Tadmor G. and Centuori M. D. (2007), "Low Order Galerkin Models for the Actuated Flow around 2-D Airfoils", AIAA-2007-1313.

Tian Y., Song Q. and Cattafesta L., (2006) "Adaptive Feedback Control of Flow Separation," AIAA-2006-3016.